Beyond Sequence: Impact of Geometric Context for RNA Property Prediction

Junjie Xu[1,2] [*] [†], **Artem Moskalev**[1] [†], **Tommaso Mansi**[1], **Mangal Prakash**[1] [‡], **Rui Liao**[1] [‡]
[1]Johnson & Johnson Innovative Medicine,
{jxu214, amoskal2, tmansi, mpraka12, rliao2}@its.jnj.com
[2]The Pennsylvania State University, junjiexu@psu.edu

Abstract

Accurate prediction of RNA properties, such as stability and interactions, is crucial for advancing our understanding of biological processes and developing RNA-based therapeutics. RNA structures can be represented as 1D sequences, 2D topological graphs, or 3D all-atom models, each offering different insights into its function. Existing works predominantly focus on 1D sequence-based models, which overlook the geometric context provided by 2D and 3D geometries. This study presents the first systematic evaluation of incorporating explicit 2D and 3D geometric information into RNA property prediction, considering not only performance but also real-world challenges such as limited data availability, partial labeling, sequencing noise, and computational efficiency. To this end, we introduce a newly curated set of RNA datasets with enhanced 2D and 3D structural annotations, providing a resource for model evaluation on RNA data. Our findings reveal that models with explicit geometry encoding generally outperform sequence-based models, with an average prediction RMSE reduction of around 12% across all various RNA tasks and excelling in low-data and partial labeling regimes, underscoring the value of explicitly incorporating geometric context. On the other hand, geometry-unaware sequence-based models are more robust under sequencing noise but often require around $2 - 5\times$ training data to match the performance of geometry-aware models. Our study offers further insights into the trade-offs between different RNA representations in practical applications and addresses a significant gap in evaluating deep learning models for RNA tasks.

1 Introduction

RNA plays a central role in the machinery of life, serving as a crucial intermediary between nucleotide and amino acid worlds [39]. Beyond its messenger role, RNA is involved in diverse biological processes, including gene regulation, catalytic activity, and structural support within ribosomes [44, 50]. This versatility makes RNA a key target for fundamental biological research and therapeutic interventions. As our understanding of RNA complexity grows, so does the need for advanced computational tools for its analysis.

Modeling RNA is challenging due to its intricate secondary and tertiary structures, dynamic conformational changes, and interactions with cellular components [19]. Furthermore, RNA analysis is hindered by the practical challenges of RNA data acquisition which include sequencing errors [33], batch effects [53], incomplete sequencing [2], partial labeling [60], and high costs of obtaining

[*] This work was done while the author was an intern at Johnson & Johnson.
[†] Equal contribution as first authors
[‡] Equal contribution as last authors

AI for New Drug Modalities at NeurIPS 2024.

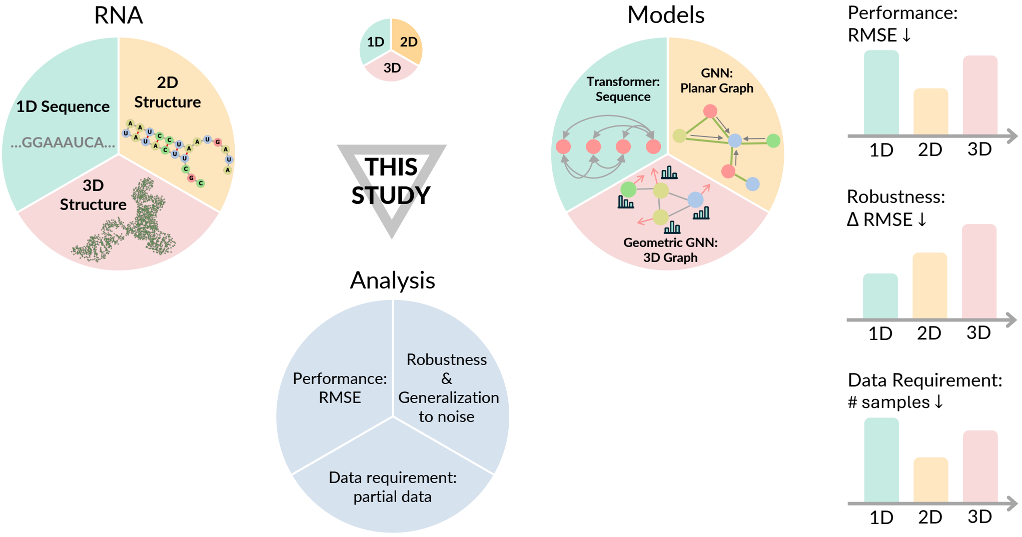

Figure 1: **Overview of the study.** (a) Left panel: RNA sequences represented in 1D, 2D, and 3D structures, processed by 1D sequence, 2D GNN, and 3D GNN models. Our analysis includes prediction error, robustness and generalization to sequencing noise, and performance under limited training data and partial labels. (b) Right panel: Comparative performance of 1D, 2D, and 3D methods across experimental conditions. Histograms show RMSE performance, relative RMSE changes with increasing noise, and data requirements for optimal performance. Lower values indicate better performance in all metrics.

large labeled datasets [7]. Moreover, RNA molecules can be represented in different ways: as a 1D nucleotide sequence, a 2D graph of base pairings, or a 3D atomic structure. Each representation highlights different aspects of RNA, presenting both opportunities and challenges for model design and selection (Fig. 1).

In this work, we systematically study the performance of various machine learning models for RNA property prediction, extending beyond traditional sequence-based approaches [20, 49, 15] to include methods that process RNA with its 2D or 3D geometry. While 2D and 3D RNA representations offer potentially richer information, they also present unique challenges. In the absence of high-quality experimental data, accessing 2D or 3D RNA structures requires running structure prediction algorithms prone to noise and mistakes, especially in the presence of sequencing errors [41, 57]. A few mutations in the nucleotide sequence owing to sequencing mistakes can hugely alter the 2D and 3D structure (Fig. 4), potentially undermining the benefit of using additional geometric context. Furthermore, real-world RNA datasets often suffer from partial labeling [60] and scarcity of training samples [62], which may affect geometry-aware methods differently than sequence-based approaches. These challenges raise a fundamental question: to what extent does explicit 2D and 3D geometry contribute to RNA property prediction, and under what circumstances might it offer advantages over geometry-free sequence models?

In this study, we seek to answer this question by making the following contributions:

- We introduce a diverse collection of RNA datasets, including newly annotated 2D and 3D structures, covering various prediction tasks at nucleotide and sequence levels across multiple species.
- We provide a unified testing environment to evaluate different types of machine learning models for RNA property prediction, including sequence models for 1D, graph neural networks for 2D, and equivariant geometric networks for 3D RNA representations.
- We conduct a comprehensive analysis of how different models perform under various conditions, such as limited data and labels, different types of sequencing errors, and out-of-distribution scenarios. We highlight the trade-offs and contexts in which each modeling approach is most effective, guiding researchers in selecting suitable models for specific RNA analysis challenges.

- We also introduce novel modifications to existing 3D geometric models based on biological prior, specifically optimizing them for handling large-scale point cloud RNA data, thus improving the efficiency and performance of 3D models significantly.

Our study reveals several key insights: **(i)** 2D models generally outperform 1D models, with spectral GNNs reducing prediction error by about 12% on average across all datasets, highlighting the importance of explicitly considering RNA structural information; **(ii)** 3D equivariant GNNs outperform 1D and some 2D methods in the noise-free scenario but are sensitive to noise, exhibiting up to a 56% decrease in prediction quality under high sequencing error rates; **(iii)** geometry-free sequence models remain the most robust to sequencing noise, showing only a 14-27% increase in prediction error compared to noise-free conditions, however, they require around $2-5\times$ more training data to match the performance of geometry-aware models.

2 Datasets and Models

Here, we discuss datasets selected for our study with RNA-level prediction labels. These datasets are selected to vary from small to large-scale and to encompass both nucleotide-level tasks and sequence-level tasks. We perform an extensive evaluation across these datasets, leveraging three different model families (1D, 2D, 3D) spanning 9 representative models in total.

2.1 Datasets

The datasets vary in size based on the number of sequences and sequence lengths: the small dataset Tc-Riboswitches [17], the medium datasets Open Vaccine COVID-19 [60] and Ribonanza-2k [22], and the large dataset Fungal [62]. All datasets provide regression labels. Detailed statistics for these datasets are provided in Appendix C.1.

1. **Tc-Riboswitches**: 355 mRNA sequences (67-73 nucleotides) with sequence-level labels for tetracycline-dependent riboswitch switching behavior, important for optimizing gene regulation in synthetic biology and gene therapy.
2. **Open Vaccine COVID-19**: 4,082 RNA sequences (each of 107 nucleotides) with nucleotide-level degradation rate labels, crucial for predicting RNA stability in mRNA vaccine development.
3. **Ribonanza-2k**: 2,260 RNA sequences (each of 120 nucleotides) with nucleotide-level experimental reactivity labels, supporting RNA structure modeling and RNA-based drug design.
4. **Fungal**: 7,056 coding and tRNA sequences (150-3,000 nucleotides) from 450 fungal species, used for sequence-level protein expression prediction.

2.2 Data Preprocessing and Curation

For the OpenVaccine COVID-19 dataset, we filter out sequences with a signal-to-noise ratio (SNR) below 1, as recommended by the dataset authors [60], to ensure that only sequences with a significant signal relative to background noise are included, thereby enhancing the reliability of modeling. For the other datasets, we use the original sequences since no SNR annotations are available.

Since all the RNA datasets come with sequences only, we employ EternaFold [59] and RhoFold [45] to infer 2D and 3D molecular structures respectively. We selected EternaFold and RhoFold due to their state-of-the-art performances acknowledged in recent works [58, 60, 22] Additionally, RhoFold typically runs in seconds to a minute per sequence, unlike other 3D structure prediction tools which usually take hours, and hence not suitable for large datasets.

For 1D modeling, we use the original RNA sequences without structural augmentation which equates to processing a plain string of nucleotides. The 2D datasets represent each RNA sequence as a graph with nodes for nucleotides and edges for bonds between nucleotides. The node features are six-dimensional, incorporating one-hot nucleotide identity (‘A’, ‘C’, ‘G’, ‘U’) alongside the sum and mean base-pairing probabilities (BPP), which are available from 2D structure prediction tools. In 3D, each RNA molecule is represented as a graph, with nodes corresponding to individual atoms. Node features represent one-hot atom identity.

2.3 Models

We select well-established model architectures recognized for their state-of-the-art performance for molecular property prediction tasks in various domains. **1D Model**: Transformer1D [24, 20]; **2D Models**: GCN [27, 61], GAT [55, 67], ChebNet [11, 28], Transformer1D2D [21], Graph Transformer [47, 31], and GraphGPS [38, 70]; **3D Models**: SchNet [42, 18] and EGNN [40].

1. **Transformer1D**: The Transformer1D model is a standard Transformer architecture adopted for RNA sequence processing. It includes an embedding layer to convert input tokens into dense vectors, positional encoding (PE) to retain sequence order, and a multi-layer Transformer encoder to capture long-range dependencies within the sequence.
2. **Transformer1D2D**: An adaptation of Transformer1D that integrates sequence and 2D graph structure information. The model encodes each nucleotide and incorporates BPP features, combining standard Transformer with positional encoding and a convolutional layer on the graph adjacency matrix. This convolutional output is added to the attention matrix, enabling the model to capture both sequential and structural dependencies.
3. **Graph Convolutional Network (GCN)**: A basic model in graph learning that aggregates and processes node features from local neighborhoods to capture both node characteristics and graph structure, making it effective for tasks like node classification.
4. **Graph Attention Network (GAT)**: Enhances graph convolutions by assigning different importance to neighboring nodes through local attention mechanisms, allowing the model to focus on more relevant nodes during feature aggregation.
5. **ChebNet**: A spectral GNN that utilizes Chebyshev polynomials to approximate the graph Laplacian, enabling graph convolutions with global structural context. This approach allows ChebNet to approximate global graph features with lower computational complexity.
6. **Graph Transformer**: This model uses Laplacian positional encoding to integrate structural information from the graph's Laplacian into node features, which are then processed by Transformer layers. This enables aligning the sequential nature of transformer layers with graph topology.
7. **GraphGPS**: A hybrid model combining GNNs with transformers to capture both local and global graph information. It uses GNNs for local feature aggregation and transformers for long-range dependencies, making it effective for complex graph tasks requiring both local and global context.
8. **SchNet**: An SE(3)-invariant network designed for molecular property prediction on geometric graphs of atomic systems. It operates by modeling interactions through continuous-filter convolutional layers. Since the continuous-filter in Schnet is conditioned on distance features, it maintains invariance to rotations and translations of atom coordinates.
9. **E(n)-Equivariant Graph Neural Network (EGNN)**: An equivariant network for geometric graphs with rotations, translations, and reflections symmetry. The EGNN operates by as a non-linear message passing between scalar-invariant and vector equivariant quantities.

Training and evaluation All models were trained on a NVIDIA A100 GPU. To ensure hyperparameter parity for each baseline, hyperparameters were optimized using Optuna [1], restricting the search to models with fewer than 10 million parameters that fit within the GPU memory constraint of 80GB. All model hyperparameters, training, and evaluation details are reported in Appendix E. We ran all models for 5 random data splits (train:val:test split of 70:15:15) and we report average performance with a standard deviation across splits. The mean column-wise root mean squared error (MCRMSE), introduced in [58], is used as the evaluation metric. It is defined as $\text{MCRMSE}(f, D) = \sqrt{\frac{1}{n}\sum_{i=1}^{n}\left(\hat{y}_i - y_i\right)^2}$, where f represents a model, D is the dataset, and $\hat{y}_i$ and y_i are the predicted and true values for data point i.

3 Task Definitions

Here, we introduce the downstream tasks for evaluating models for RNA property prediction. Each task is designed to quantify specific behaviors under various real-world experimental conditions.

Task 1: Impact of structural information on prediction performance This task aims to evaluate how incorporating RNA structural information affects prediction quality. We compare the performance of models using 1D (sequence-only), 2D, and 3D RNA representations to determine if and to what extent geometric data improves property prediction.

Task 2: Model efficiency in limited training data settings Acquiring high-quality comprehensive RNA datasets is often challenging and resource-intensive thus limiting the amount of labeled data for training [51, 7]. This task aims to investigate how model performance depends on the amount of training data used, evaluating the sample efficiency of each family of models. In other words, given a dataset $D = \{X, Y\}$, let $D_\alpha = \{X_\alpha, Y_\alpha\}$ be a subset where the training set is reduced to a fraction α. We train models on different sets of D_α datasets with decreasing α.

Task 3: Performance with partial sequence labeling Due to the high cost of measuring properties for every nucleotide in RNA sequence, real-world datasets often contain partial annotations [60] where labels are only available for the first small part of the sequence. This task is relevant for nucleotide-level datasets and it aims to investigate how well a model can generalize to a whole RNA sequence when labels are only available for a portion of it.

Task 4: Robustness to sequencing noise Acquiring RNA data requires sequencing. In practice sequencing procedures may introduce sequencing errors (random mutations of nucleotides) that vary depending on the sequencing technology and platform [33, 14]. These errors affect the raw sequence data and propagate to structural noise in 2D and 3D. The goal of this task is to assess how well models can maintain reliable performance when trained and tested under the same distribution of realistic levels of sequencing noise observed in practice, ensuring robustness across a consistent noise environment. This reflects real-world cases where a specific sequencing method produces noisy data, but the noise characteristics are stable across training and deployment.

Task 5: Generalization to Out-of-Distribution (OOD) data This task focuses on a different practical challenge: models trained on high-quality RNA sequences are often deployed in conditions where the data exhibits different noise characteristics due to batch effect [53] or the use of different sequencing platforms [52]. Here, the objective is to evaluate how well models generalize to OOD datasets with different levels of sequencing noise, assessing the extent of performance degradation as noise levels increase. This task simulates the scenario where a model encounters noisier data than it was trained on, highlighting its ability to adapt to unexpected experimental conditions.

4 Experiments and Results

4.1 Impact of explicit geometry learning on model performance

We begin by addressing Task 1, where we compare the performance of model families when trained and evaluated on the downstream RNA datasets. Additionally, we provide runtime and memory comparison in Appendix B.

2D models consistently outperform 1D model Results in Table 1 reveal that 2D methods consistently outperform the 1D sequence model across all datasets. Notably, the Transformer1D2D model, which simply augments the attention matrix with adjacency features alongside, achieves around 10% lower prediction MCRMSE on average across datasets than its geometry-free counterpart. This suggests that explicitly incorporating structural information is crucial, as learning from sequence data alone proves to be insufficient. Further experiments, detailed in the Appendix C.4, investigate the learned attention maps of both the Transformer1D2D and the Transformer1D model and their correlation with structural information and reveal that Transformer1D2D attention maps are much more closely aligned with the topological structure of nucleotide graph, reinforcing the conclusion that explicit encoding of structural information is essential for improved performance.

Spectral GNN outperforms spatial GNNs in 2D ChebNet, a spectral method, outperforms spatial methods such as GCN, GAT, Graph Transformer, and GraphGPS, achieving a prediction MCRMSE 2.5% lower than the next best 2D model across datasets. Spatial GNNs aggregate node

Table 1: **Comparison of 1D, 2D, and 3D models across datasets. Bold** indicates the best, underline the second-best. 'OOM' means out-of-memory. ChebNet excels by capturing global graph information. Overall, 2D models outperform 1D models, highlighting the value of structural information. Although 3D models face challenges with scalability and noisy predictions, our nucleotide pooling strategy, based on biological prior, enhances their performance on shorter sequences, allowing 3D encoding to occasionally surpass 1D models. See Sec. 4.1 for details on nucleotide pooling strategy.

Model	**COVID**	**Ribonanza**	**Tc-Ribo**	**Fungal**
1D model				
Transformer1D	0.361±0.017	0.705±0.015	0.705±0.079	1.417±0.005
2D model				
Transformer1D2D	0.305±0.012	0.514±0.004	0.633±0.001	OOM
GCN	0.359±0.009	0.595±0.006	0.701±0.004	1.192±0.077
GAT	0.315±0.006	0.534±0.006	0.685±0.024	1.112±0.035
ChebNet	**0.279±0.007**	**0.468±0.002**	**0.621±0.022**	**0.973±0.003**
Graph Transformer	0.318±0.008	0.515±0.001	0.710±0.041	1.317±0.002
GraphGPS	0.332±0.013	0.523±0.003	0.715±0.012	1.025±0.081
3D model				
EGNN (w/o pooling)	0.480±0.025	0.808±0.023	0.725±0.002	OOM
SchNet (w/o pooling)	0.499±0.003	0.843±0.004	0.696±0.008	OOM
EGNN (nuc. pooling)	0.364±0.003	0.619±0.007	0.663±0.010	OOM
SchNet (nuc. pooling)	0.390±0.006	0.685±0.006	0.655±0.038	OOM

features layer by layer, emphasizing local information within a fixed distance. While computationally efficient, these methods are limited by the 1-Weisfeiler-Lehman (WL) test, which constrains the expressive power of node-based updates [63]. In addition, spatial GNNs may suffer from a limited receptive field while spectral methods approximate global graph features, enabling a global receptive field since the first layer. This allows ChebNet to effectively process global information which is important for RNA data due to potential long-range interaction between nucleotides.

Challenges of modeling geometric context in all-atom resolution Contrary to our expectations, 3D models at all-atom resolution (EGNN w/o pooling and SchNet w/o pooling in Table 1) show relatively high prediction MCRMSE across datasets, underperforming compared to 1D and 2D methods. We hypothesize this is due to two factors.

First, all-atom SchNET and EGNN rely on a limited local neighborhood of adjacent atoms, limiting their receptive fields and preventing them from capturing long-range dependencies (see Appendix Table C.1), which can be crucial for determining RNA properties [46, 3]. Expanding the local neighborhood for these methods turns challenging due to the overwhelming scale of large molecular systems in all-atom resolution. Second, the performance of 3D models is often limited by the inherent inaccuracies in 3D structure prediction tools, which are generally less reliable compared to 2D structure prediction methods [37].

To address the receptive field limitation of all-atom methods, we employ a biological prior by pooling atomic features into nucleotide-level representations after a few layers of all-atom operations. This strategy is aligned with RNA's natural secondary structure, where atoms group into nucleotides, and nucleotides form the complete RNA molecule [12]. This novel strategy allows us to maintain all-atom resolution in the initial layers while increasing the receptive field via pooling. By balancing the number of all-atom and nucleotide layers as hyperparameters, we can balance fine- and coarse-grained all-atom and nucleotide resolution. We call 3D models with pooling EGNN (nuc. pooling) and SchNet (nuc. pooling). This strategy significantly enhances 3D model performance, reducing prediction MCRMSE by $\sim$10% compared to the original EGNN and SchNet, and outperforming 1D models on the Ribonanza-2k and Tc-Riboswitches datasets by 5% on average. On the COVID dataset, EGNN (nuc. pooling) matches the Transformer1D model but still trails behind 2D models. All subsequent experiments report results using nucleotide-pooled versions of the 3D models.

Next, we investigated the second hypothesis regarding higher noise in 3D structures by quantifying variability in predicted structures across different 3D prediction tools in Appendix D. We observe substantial variability (between 11-45Å RMSD across structures given by different 3D structure prediction tools), suggesting considerable noise in 3D predictions, which likely contributes to the poorer performance of 3D models.

4.2 Model efficiency under limited data and partial sequence labeling

In this section, we combine the analysis of Tasks 2 and 3, assessing model performance in scenarios with limited training data or partial labels.

To analyze how the amount of training data influences model performance, we run experiments with varying portions of the full datasets (25%, 50%, 75%, and 100%) on the medium- and large-scale datasets: COVID, Ribonanza-2k, and Fungal (Appendix Fig. 8(a) for illustration). The small size of the Tc-Riboswitches dataset is excluded from the analysis, as training with lower ratios would have resulted in inadequate sample sizes for meaningful evaluation. Additionally, GPU memory constraints prevent the application of Transformer1D2D and 3D models on the Fungal dataset due to its large sequence length.

We also evaluate the impact of partial property labels for nucleotide-level tasks, a common occurrence owing to costly experimental measurements [58] to identify which models are best suited to handle the challenges of incomplete labels in RNA property prediction. For this, we use the COVID and Ribonanza datasets as these datasets contain nucleotide-level labels. We train the models using all training data but with varying proportions of labeled nucleotides (20%, 40%, 60%, 80%, and 100%) per sequence, thus simulating incomplete or sparse labeling, while testing on fully labeled test sets (Appendix Fig. 8(b) for illustration).

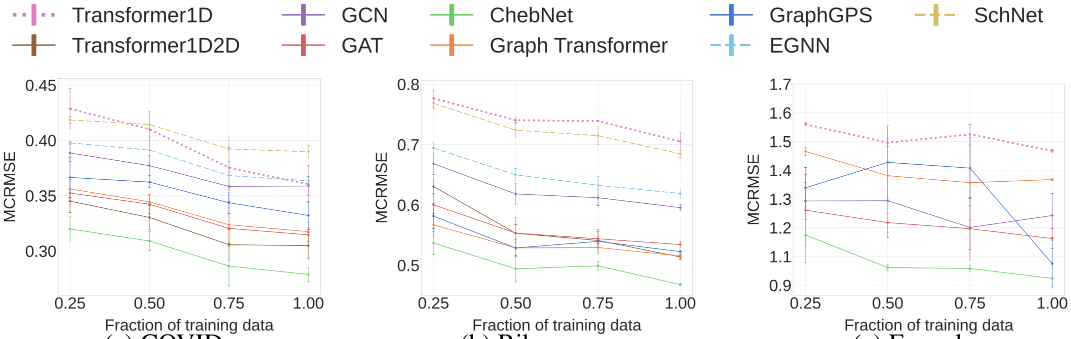

(a) COVID (b) Ribonanza (c) Fungal

Figure 2: **Performance versus fraction of training data across various datasets.** Model performance improves with increasing data, with lower MCRMSE across all models. 2D models consistently outperform 1D models, particularly in low-data regimes, underscoring the value of structural information for generalization. Dotted, solid, and dashed lines denote 1D, 2D, and 3D methods, respectively, which apply consistently throughout all figures in this paper.

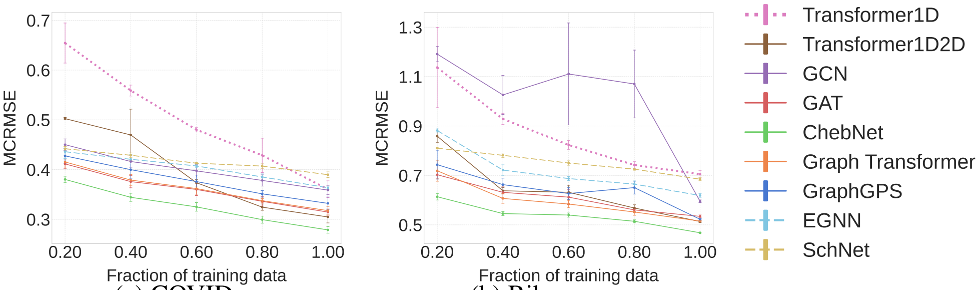

(a) COVID (b) Ribonanza

Figure 3: **Performance vs. partial property labels on COVID and Ribonanza datasets.** 2D models consistently outperform 1D models with sparse labeling, while Transformer1D and Transformer1D2D improve rapidly with denser supervision, emphasizing the need for more labels in transformer-based models.

More training data improves performance Unsurprisingly, across all models and datasets, a clear trend emerges: increasing the amount of available data, whether through higher number of training data points or greater proportion of available labels leads to improved performance (Fig. 2, Fig. 3, Appendix Tables in Sec. F.1, F.2). However, the degree of performance improvement varies significantly between model types, as analyzed next.

2D models excel in low data and partial label regimes Evaluating model performance at different training and label ratios reveals a notable trend: 2D models consistently outperform 1D and 3D models under low data and incomplete labeling regimes. Between 20-50% training data and label levels, 2D models such as ChebNet, Transformer1D2D, GraphGPS, and GAT significantly outperform Transformer1D, highlighting the role of additional structural information for model sample efficiency. Interestingly, Transformer1D and Transformer1D2D exhibit a faster rate of improvement when more labels are available (Fig. 3), suggesting that transformer-based architectures benefit from denser supervision. Notably, Transformer1D requires $2-5\times$ more training data/labels to match the performance of the least effective 2D models, which achieve comparable results using only 20% to 50% of the training data needed by Transformer1D when trained on the full dataset.

3D models outperform 1D model in limited data regime despite structural noise For the medium-scale datasets (COVID and Ribonanza), where 3D models can be evaluated, we observe that the 3D models generally outperform or are on par with the Transformer1D, even for lower data and labeling regimes. This suggests that despite the noise introduced by inaccuracies in 3D structure predictions, the explicit geometric encoding in 3D models still provides an advantage over 1D models. EGNN, in particular, is consistently better than or on par with Transformer1D across all training and label ratios. This further emphasizes that models incorporating explicit geometric encoding (whether 2D or 3D) are more data-efficient than those relying solely on sequence information. However, it is important to note that 3D models do not match the efficiency of 2D models in these scenarios, likely due to their susceptibility to noise as discussed in Section 4.1.

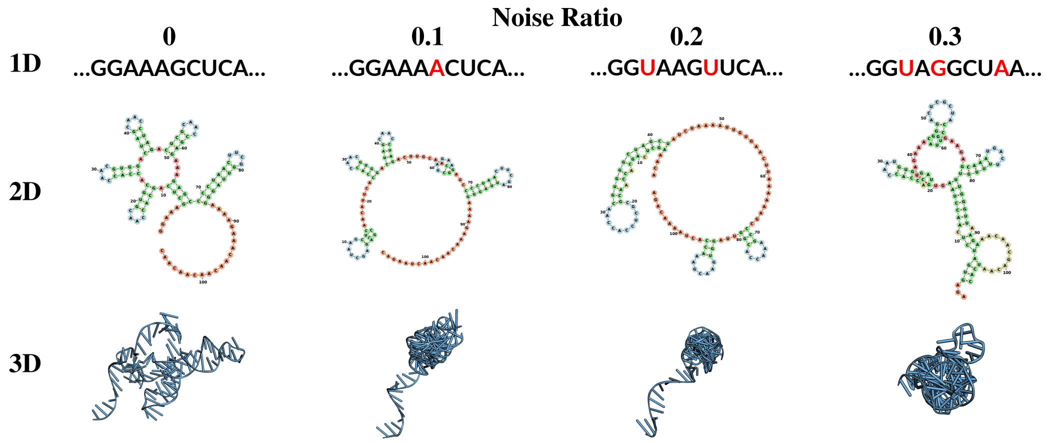

Figure 4: **Visualization of 1D, 2D, and 3D structures under varying noise ratios (mutation errors during sequencing).** Each column represents a different noise ratio, showcasing the impact of noise on the structures across different dimensions.

4.3 Model Robustness and Generalization Under Sequencing Noise

Tasks 4 and 5 both deal with model performance with noise in the data, but focus on different aspects, robustness to noise, and ability to generalize across unseen noise distributions. As explained in Sec. 3, sequencing noise is common depending on the sequencing method and platform used [14], thereby introducing errors in sequences that propagate into 2D and 3D structures. Additionally one of the deployment scenarios involves models trained on high-quality clean data applied for datasets acquired under noisy conditions owing to different sequencing platforms or experimental batch effects [52].

To explore these practical aspects, we design two sets of experiments:

- *Robustness:* We introduce sequencing noise into the training, validation, and test sequences to simulate realistic sequencing errors. Nucleotide mutations are applied with probabilities {0.05, 0.1, 0.15, 0.2, 0.25, 0.3}, mirroring typical sequencing error rates [36] which also propagates to the 2D and 3D structures (Fig. 4) via structure prediction tools. Importantly, these mutations are not random; the likelihood of a particular nucleotide mutating into another varies, as is well documented in sequencing studies [36]. Our noise model reflects these real-world mutation profiles. Crucially, while the input training, validation, and test sequences contain noise, the property labels remain clean. This again reflects practical scenarios where labels are experimentally determined independent of sequencing and thus unaffected by sequencing errors.
- *Generalization:* Here, models are trained on clean, noise-free data corresponding to high-quality sequencing experiments but are tested on datasets with varying levels of noise simulated by sequencing mutation probabilities in {0.05, 0.1, 0.15, 0.2, 0.25, 0.3}. This setup reflects the real-world scenario where models trained on high-quality data will be deployed on OOD data that may come from different sequencers or have been affected by batch effects.

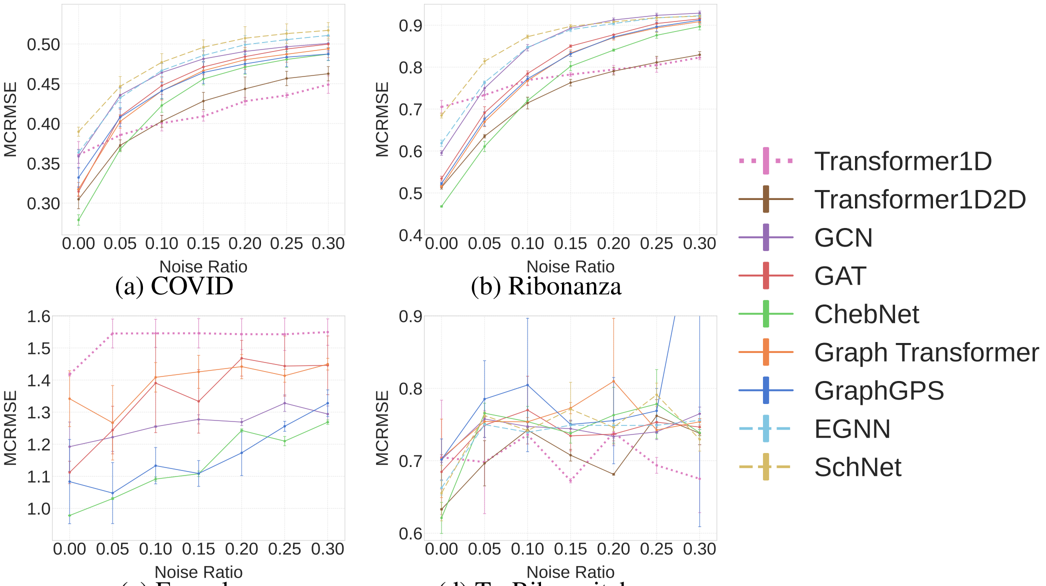

(a) COVID (b) Ribonanza

(c) Fungal (d) Tc-Riboswitches

Figure 5: **Robustness experiments.** Transformer1D shows the least performance drop under increasing noise, maintaining the highest accuracy, with Transformer1D2D following closely. In contrast, 2D and 3D models, particularly ChebNet and 3D models, are more impacted by noise.

Transformer architectures demonstrate superior robustness and generalization under sequencing noise Expectedly, across both tasks, increased noise levels generally lead to worse test MCRMSE for all models, indicating a decline in prediction performance (Fig. 5, Fig. 6 and Appendix Tables in Sec. F.3, F.4).

Among all models, Transformer1D demonstrates the highest robustness and generalization, exhibiting the least performance degradation as noise levels increase. Notably, in generalization experiments, Transformer1D achieves the best prediction MCRMSE on the COVID, Ribonanza, and Tc-Riboswitches datasets under higher noise levels (Fig. 6 and Appendix F.4). The reliance of Transformer1D on sequence-only information without considering geometric context, while being a weakness in other scenarios, becomes a strength in case of noisy sequences as minor sequencing errors may severely alter the predicted RNA structures (Fig. 4). While its performance on the Fungal dataset is worse overall, Transformer1D maintains remarkably consistent performance as noise increases. Transformer1D2D ranks just behind Transformer1D outperforming other 2D and 3D models. This can be attributed to Transformer1D2D's ability to selectively focus on sequence information for noisy data rather than relying on structural data alone as the self-attention is only weakly conditioned on the graph topology.

More elaborated 2D and 3D models, which rigidly rely on structural information, are significantly more affected by noise, underperforming compared to plain sequence baseline in both robustness

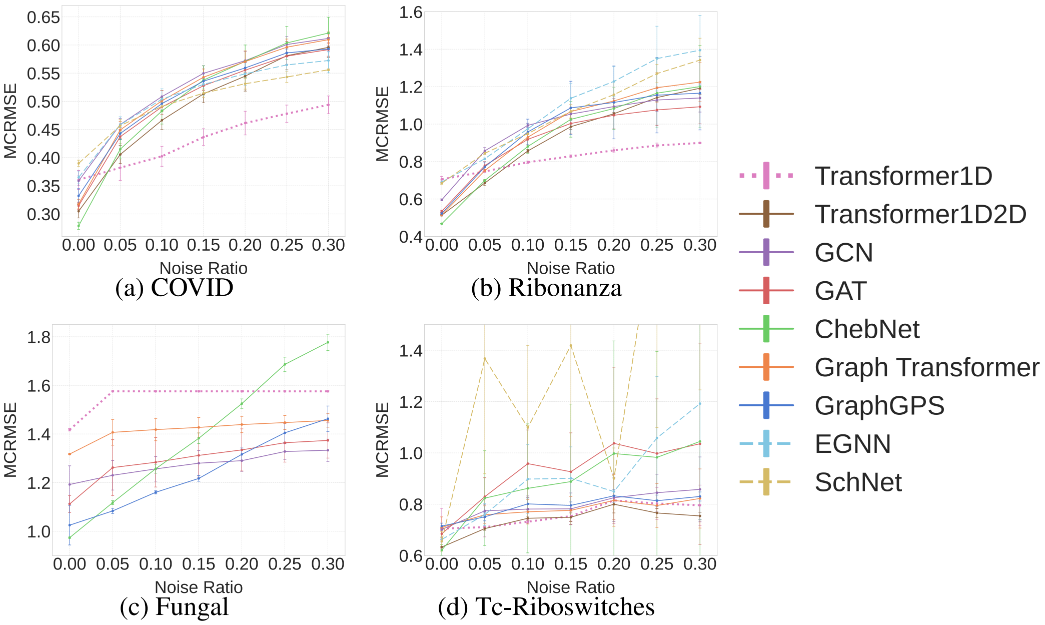

(a) COVID

(b) Ribonanza

(c) Fungal

(d) Tc-Riboswitches

Figure 6: **Generalization experiments.** Transformer1D outperforms other models on noisy sequences, achieving the lowest RMSE at higher noise levels, particularly on COVID, Ribonanza, and Tc-Riboswitches. Transformer1D2D follows closely, showing that transformer-based models generalize better under noise than 2D and 3D models, especially in tasks with geometric representations.

and generalization experiments. Interestingly, ChebNet shows the worst generalization among 2D models, although it performs on par with other methods in robustness experiments. This suggests that while ChebNet struggles with OOD noise, its performance gets better when it is also trained on the same noise level used during testing, highlighting the need for retraining for different experimental data batches/noise levels in real-world applications. Across both experiments, 3D models have poor performance for more noisy conditions, particularly with the COVID and Ribonanza datasets, due to their dependence on 3D structures which are also sensitive to the propagation of sequencing errors (Fig.4 bottom). In the smaller Tc-Riboswitches dataset, model performances vary more, likely due to limited data size, but transformer models still consistently demonstrate greater robustness to noise.

Across both settings, as the noise ratio rises, the 1D model demonstrates the greatest resilience to noise, showing an average test MCRMSE increase of approximately 14% and 27%, respectively, relative to the train and test on clean data. In contrast, 2D models exhibit the highest sensitivity, with test MCRMSE increasing from 30% to 82%. Meanwhile, 3D models show intermediate performance, with MCRMSE increases of 29% and 56%. Our results reveal a higher vulnerability of 2D and 3D models to sequencing noise where geometric context becomes unreliable at a faster rate than a plain sequence of nucleotides.

5 Conclusion

We present the first comprehensive study on the benefits and challenges of the effect of geometric context for RNA property prediction models. By providing a curated set of RNA datasets with annotated 2D and 3D structures, we systematically evaluate the performance of 1D, 2D, and 3D models under various real-world conditions, such as limited data, partial labeling, sequencing errors, and out-of-distribution generalization. Our results reveal that 2D models outperform 1D and 3D models, with spectral graph neural networks excelling even in low-data and partial labeling scenarios. For 3D models, we find that their potential benefits are hindered by the limited receptive field, computational complexity, and structural noise from RNA structure prediction tools. At the same time, 1D models demonstrate better robustness compared to 2D and 3D models in noisy and OOD conditions. This study highlights the value and limitations of using geometric context for RNA modeling. Future work could focus on ensembling 1D, 2D, and 3D models for complementary strengths, and on improving 2D and 3D models to better handle noise from structure prediction tools.

References

[1] Takuya Akiba, Shotaro Sano, Toshihiko Yanase, Takeru Ohta, and Masanori Koyama. Optuna: A next-generation hyperparameter optimization framework. In *Proceedings of the 25th ACM SIGKDD international conference on knowledge discovery & data mining*, pages 2623–2631, 2019.

[2] Juan D Alfonzo, Jessica A Brown, Peter H Byers, Vivian G Cheung, Richard J Maraia, and Robert L Ross. A call for direct sequencing of full-length rnas to identify all modifications. *Nature genetics*, 53(8):1113–1116, 2021.

[3] Ibraheem Alshareedah, Taranpreet Kaur, Jason Ngo, Hannah Seppala, Liz-Audrey Djomnang Kounatse, Wei Wang, Mahdi Muhammad Moosa, and Priya R Banerjee. Interplay between short-range attraction and long-range repulsion controls reentrant liquid condensation of ribonucleoprotein–rna complexes. *Journal of the American Chemical Society*, 141(37):14593–14602, 2019.

[4] Viplove Arora and Guido Sanguinetti. De novo prediction of rna–protein interactions with graph neural networks. *RNA*, 28(11):1469–1480, 2022.

[5] Minkyung Baek, Ryan McHugh, Ivan Anishchenko, Hanlun Jiang, David Baker, and Frank DiMaio. Accurate prediction of protein–nucleic acid complexes using rosettafoldna. *Nature methods*, 21(1):117–121, 2024.

[6] Michal J Boniecki, Grzegorz Lach, Wayne K Dawson, Konrad Tomala, Pawel Lukasz, Tomasz Soltysinski, Kristian M Rother, and Janusz M Bujnicki. Simrna: a coarse-grained method for rna folding simulations and 3d structure prediction. *Nucleic acids research*, 44(7):e63–e63, 2016.

[7] Sara A Byron, Kendall R Van Keuren-Jensen, David M Engelthaler, John D Carpten, and David W Craig. Translating rna sequencing into clinical diagnostics: opportunities and challenges. *Nature Reviews Genetics*, 17(5):257–271, 2016.

[8] Jiayang Chen, Zhihang Hu, Siqi Sun, Qingxiong Tan, Yixuan Wang, Qinze Yu, Licheng Zong, Liang Hong, Jin Xiao, Tao Shen, et al. Interpretable rna foundation model from unannotated data for highly accurate rna structure and function predictions. *arXiv preprint arXiv:2204.00300*, 2022.

[9] Xinshi Chen, Yu Li, Ramzan Umarov, Xin Gao, and Le Song. Rna secondary structure prediction by learning unrolled algorithms. *arXiv preprint arXiv:2002.05810*, 2020.

[10] Rhiju Das and David Baker. Automated de novo prediction of native-like rna tertiary structures. *Proceedings of the National Academy of Sciences*, 104(37):14664–14669, 2007.

[11] Michaël Defferrard, Xavier Bresson, and Pierre Vandergheynst. Convolutional neural networks on graphs with fast localized spectral filtering. In *Advances in Neural Information Processing Systems*, pages 3844–3852, 2016.

[12] Jie Deng, Xianyang Fang, Lin Huang, Shanshan Li, Lilei Xu, Keqiong Ye, Jinsong Zhang, Kaiming Zhang, and Qiangfeng Cliff Zhang. Rna structure determination: From 2d to 3d. *Fundamental Research*, 3(5):727–737, 2023.

[13] Matthias Fey and Jan E. Lenssen. Fast graph representation learning with PyTorch Geometric. In *ICLR Workshop on Representation Learning on Graphs and Manifolds*, 2019.

[14] Edward J Fox, Kate S Reid-Bayliss, Mary J Emond, and Lawrence A Loeb. Accuracy of next generation sequencing platforms. *Next generation, sequencing & applications*, 1, 2014.

[15] Jörg Franke, Frederic Runge, and Frank Hutter. Probabilistic transformer: Modelling ambiguities and distributions for rna folding and molecule design. *Advances in Neural Information Processing Systems*, 35:26856–26873, 2022.

[16] Laiyi Fu, Yingxin Cao, Jie Wu, Qinke Peng, Qing Nie, and Xiaohui Xie. Ufold: fast and accurate rna secondary structure prediction with deep learning. *Nucleic acids research*, 50(3):e14–e14, 2022.

[17] Ann-Christin Groher, Sven Jager, Christopher Schneider, Florian Groher, Kay Hamacher, and Beatrix Suess. Tuning the performance of synthetic riboswitches using machine learning. *ACS synthetic biology*, 8(1):34–44, 2018.

[18] Jiaqi Han, Yu Rong, Tingyang Xu, and Wenbing Huang. Geometrically equivariant graph neural networks: A survey. *arXiv preprint arXiv:2202.07230*, 2022.

[19] Yixing Han, Shouguo Gao, Kathrin Muegge, Wei Zhang, and Bing Zhou. Advanced applications of rna sequencing and challenges. *Bioinformatics and biology insights*, 9:BBI–S28991, 2015.

[20] Shujun He, Baizhen Gao, Rushant Sabnis, and Qing Sun. Nucleic transformer: Deep learning on nucleic acids with self-attention and convolutions. *bioRxiv*, pages 2021–01, 2021.

[21] Shujun He, Baizhen Gao, Rushant Sabnis, and Qing Sun. Rnadegformer: accurate prediction of mrna degradation at nucleotide resolution with deep learning. *Briefings in Bioinformatics*, 24(1):bbac581, 2023.

[22] Shujun He, Rui Huang, Jill Townley, Rachael C Kretsch, Thomas G Karagianes, David BT Cox, Hamish Blair, Dmitry Penzar, Valeriy Vyaltsev, Elizaveta Aristova, et al. Ribonanza: deep learning of rna structure through dual crowdsourcing. *bioRxiv*, 2024.

[23] Ivo L Hofacker, Walter Fontana, Peter F Stadler, L Sebastian Bonhoeffer, Manfred Tacker, Peter Schuster, et al. Fast folding and comparison of rna secondary structures. *Monatshefte fur chemie*, 125:167–167, 1994.

[24] Shion Honda, Shoi Shi, and Hiroki R Ueda. Smiles transformer: Pre-trained molecular fingerprint for low data drug discovery. *arXiv preprint arXiv:1911.04738*, 2019.

[25] Chaitanya K. Joshi, Cristian Bodnar, Simon V. Mathis, Taco Cohen, and Pietro Liò. On the expressive power of geometric graph neural networks. In *International Conference on Machine Learning*, 2023.

[26] Wolfgang Kabsch. A solution for the best rotation to relate two sets of vectors. *Acta Crystallographica Section A: Crystal Physics, Diffraction, Theoretical and General Crystallography*, 32(5):922–923, 1976.

[27] Thomas N Kipf and Max Welling. Semi-supervised classification with graph convolutional networks. In *5th International Conference on Learning Representations, ICLR 2017, Toulon, France, April 24-26, 2017, Conference Track Proceedings*, 2017.

[28] Boris Knyazev, Xiao Lin, Mohamed R Amer, and Graham W Taylor. Spectral multigraph networks for discovering and fusing relationships in molecules. *arXiv preprint arXiv:1811.09595*, 2018.

[29] Sowmya R Krishnan, Arijit Roy, and M Michael Gromiha. Reliable method for predicting the binding affinity of rna-small molecule interactions using machine learning. *Briefings in Bioinformatics*, 25(2):bbae002, 2024.

[30] Mandar Kulkarni, Jayaraman Thangappan, Indrajit Deb, and Sangwook Wu. Comparative analysis of rna secondary structure accuracy on predicted rna 3d models. *Plos one*, 18(9):e0290907, 2023.

[31] Han Li, Dan Zhao, and Jianyang Zeng. Kpgt: knowledge-guided pre-training of graph transformer for molecular property prediction. In *Proceedings of the 28th ACM SIGKDD Conference on Knowledge Discovery and Data Mining*, pages 857–867, 2022.

[32] Chandran Nithin, Sebastian Kmiecik, Roman Błaszczyk, Julita Nowicka, and Irina Tuszyńska. Comparative analysis of rna 3d structure prediction methods: towards enhanced modeling of rna–ligand interactions. *Nucleic Acids Research*, 52(13):7465–7486, 2024.

[33] Fatih Ozsolak and Patrice M Milos. Rna sequencing: advances, challenges and opportunities. *Nature reviews genetics*, 12(2):87–98, 2011.

[34] Robin Pearce, Gilbert S Omenn, and Yang Zhang. De novo rna tertiary structure prediction at atomic resolution using geometric potentials from deep learning. *BioRxiv*, pages 2022–05, 2022.

[35] Rafael Josip Penić, Tin Vlašić, Roland G Huber, Yue Wan, and Mile Šikić. Rinalmo: General-purpose rna language models can generalize well on structure prediction tasks. *arXiv preprint arXiv:2403.00043*, 2024.

[36] Franziska Pfeiffer, Carsten Gröber, Michael Blank, Kristian Händler, Marc Beyer, Joachim L Schultze, and Günter Mayer. Systematic evaluation of error rates and causes in short samples in next-generation sequencing. *Scientific reports*, 8(1):10950, 2018.

[37] Almudena Ponce-Salvatierra, Astha, Katarzyna Merdas, Chandran Nithin, Pritha Ghosh, Sunandan Mukherjee, and Janusz M Bujnicki. Computational modeling of rna 3d structure based on experimental data. *Bioscience reports*, 39(2):BSR20180430, 2019.

[38] Ladislav Rampášek, Mikhail Galkin, Vijay Prakash Dwivedi, Anh Tuan Luu, Guy Wolf, and Dominique Beaini. Recipe for a General, Powerful, Scalable Graph Transformer. *Advances in Neural Information Processing Systems*, 35, 2022.

[39] Ugur Sahin, Katalin Karikó, and Özlem Türeci. mrna-based therapeutics—developing a new class of drugs. *Nature reviews Drug discovery*, 13(10):759–780, 2014.

[40] Vıctor Garcia Satorras, Emiel Hoogeboom, and Max Welling. E (n) equivariant graph neural networks. In *International conference on machine learning*, pages 9323–9332. PMLR, 2021.

[41] Bohdan Schneider, Blake Alexander Sweeney, Alex Bateman, Jiri Cerny, Tomasz Zok, and Marta Szachniuk. When will rna get its alphafold moment? *Nucleic Acids Research*, 51(18):9522–9532, 2023.

[42] Kristof Schütt, Pieter-Jan Kindermans, Huziel Enoc Sauceda Felix, Stefan Chmiela, Alexandre Tkatchenko, and Klaus-Robert Müller. Schnet: A continuous-filter convolutional neural network for modeling quantum interactions. *Advances in neural information processing systems*, 30, 2017.

[43] Shantanu Sharma, Feng Ding, and Nikolay V Dokholyan. ifoldrna: three-dimensional rna structure prediction and folding. *Bioinformatics*, 24(17):1951–1952, 2008.

[44] Phillip A Sharp. The centrality of rna. *Cell*, 136(4):577–580, 2009.

[45] Tao Shen, Zhihang Hu, Zhangzhi Peng, Jiayang Chen, Peng Xiong, Liang Hong, Liangzhen Zheng, Yixuan Wang, Irwin King, Sheng Wang, et al. E2efold-3d: End-to-end deep learning method for accurate de novo rna 3d structure prediction. *arXiv preprint arXiv:2207.01586*, 2022.

[46] Sumangala Shetty, Snezana Stefanovic, and Mihaela Rita Mihailescu. Hepatitis c virus rna: molecular switches mediated by long-range rna–rna interactions? *Nucleic acids research*, 41(4):2526–2540, 2013.

[47] Yunsheng Shi, Zhengjie Huang, Shikun Feng, Hui Zhong, Wenjin Wang, and Yu Sun. Masked label prediction: Unified message passing model for semi-supervised classification. *arXiv preprint arXiv:2009.03509*, 2020.

[48] Jaswinder Singh, Kuldip Paliwal, Tongchuan Zhang, Jaspreet Singh, Thomas Litfin, and Yaoqi Zhou. Improved rna secondary structure and tertiary base-pairing prediction using evolutionary profile, mutational coupling and two-dimensional transfer learning. *Bioinformatics*, 37(17):2589–2600, 2021.

[49] Necla Nisa Soylu and Emre Sefer. Bert2ome: Prediction of 2-o-methylation modifications from rna sequence by transformer architecture based on bert. *IEEE/ACM Transactions on Computational Biology and Bioinformatics*, 20(3):2177–2189, 2023.

[50] Eric J Strobel, Kyle E Watters, David Loughrey, and Julius B Lucks. Rna systems biology: uniting functional discoveries and structural tools to understand global roles of rnas. *Current opinion in biotechnology*, 39:182–191, 2016.

[51] Marc Teufel and Patrick Sobetzko. Reducing costs for dna and rna sequencing by sample pooling using a metagenomic approach. *BMC genomics*, 23(1):613, 2022.

[52] Jennifer A Tom, Jens Reeder, William F Forrest, Robert R Graham, Julie Hunkapiller, Timothy W Behrens, and Tushar R Bhangale. Identifying and mitigating batch effects in whole genome sequencing data. *BMC bioinformatics*, 18:1–12, 2017.

[53] Hoa Thi Nhu Tran, Kok Siong Ang, Marion Chevrier, Xiaomeng Zhang, Nicole Yee Shin Lee, Michelle Goh, and Jinmiao Chen. A benchmark of batch-effect correction methods for single-cell rna sequencing data. *Genome biology*, 21:1–32, 2020.

[54] Ashish Vaswani, Noam Shazeer, Niki Parmar, Jakob Uszkoreit, Llion Jones, Aidan N Gomez, Łukasz Kaiser, and Illia Polosukhin. Attention is all you need. In *Advances in Neural Information Processing Systems*, pages 5998–6008, 2017.

[55] Petar Veličković, Guillem Cucurull, Arantxa Casanova, Adriana Romero, Pietro Liò, and Yoshua Bengio. Graph attention networks. In *6th International Conference on Learning Representations, ICLR 2018, Vancouver, BC, Canada, April 30–May 3, 2018, Conference Track Proceedings*, 2018.

[56] Hong Wang, Shuyu Wang, Yong Zhang, Shoudong Bi, and Xiaolei Zhu. A brief review of machine learning methods for rna methylation sites prediction. *Methods*, 203:399–421, 2022.

[57] Wenkai Wang, Chenjie Feng, Renmin Han, Ziyi Wang, Lisha Ye, Zongyang Du, Hong Wei, Fa Zhang, Zhenling Peng, and Jianyi Yang. trrosettarna: automated prediction of rna 3d structure with transformer network. *Nature Communications*, 14(1):7266, 2023.

[58] Hannah K. Wayment-Steele, Wipapat Kladwang, and Rhiju Das. Rna secondary structure packages ranked and improved by high-throughput experiments. *bioRxiv*, 2020.

[59] Hannah K Wayment-Steele, Wipapat Kladwang, Alexandra I Strom, Jeehyung Lee, Adrien Treuille, Alex Becka, Eterna Participants, and Rhiju Das. Rna secondary structure packages evaluated and improved by high-throughput experiments. *Nature methods*, 19(10):1234–1242, 2022.

[60] Hannah K Wayment-Steele, Wipapat Kladwang, Andrew M Watkins, Do Soon Kim, Bojan Tunguz, Walter Reade, Maggie Demkin, Jonathan Romano, Roger Wellington-Oguri, John J Nicol, et al. Deep learning models for predicting rna degradation via dual crowdsourcing. *Nature Machine Intelligence*, 4(12):1174–1184, 2022.

[61] Oliver Wieder, Stefan Kohlbacher, Mélaine Kuenemann, Arthur Garon, Pierre Ducrot, Thomas Seidel, and Thierry Langer. A compact review of molecular property prediction with graph neural networks. *Drug Discovery Today: Technologies*, 37:1–12, 2020.

[62] Rhondene Wint, Asaf Salamov, and Igor V Grigoriev. Kingdom-wide analysis of fungal protein-coding and trna genes reveals conserved patterns of adaptive evolution. *Molecular biology and evolution*, 39(2):msab372, 2022.

[63] Keyulu Xu, Weihua Hu, Jure Leskovec, and Stefanie Jegelka. How powerful are graph neural networks? In *International Conference on Learning Representations*, 2018.

[64] Xiaojun Xu, Peinan Zhao, and Shi-Jie Chen. Vfold: a web server for rna structure and folding thermodynamics prediction. *PloS one*, 9(9):e107504, 2014.

[65] Zichao Yan, William L Hamilton, and Mathieu Blanchette. Graph neural representational learning of rna secondary structures for predicting rna-protein interactions. *Bioinformatics*, 36(Supplement_1):i276–i284, 2020.

[66] Yuning Yang, Gen Li, Kuan Pang, Wuxinhao Cao, Xiangtao Li, and Zhaolei Zhang. Deciphering 3'utr mediated gene regulation using interpretable deep representation learning. *bioRxiv*, pages 2023–09, 2023.

[67] Xian-bin Ye, Quanlong Guan, Weiqi Luo, Liangda Fang, Zhao-Rong Lai, and Jun Wang. Molecular substructure graph attention network for molecular property identification in drug discovery. *Pattern Recognition*, 128:108659, 2022.

[68] Yi Zhang, Jun Wang, and Yi Xiao. 3drna: Building rna 3d structure with improved template library. *Computational and structural biotechnology journal*, 18:2416–2423, 2020.

[69] Jingjing Zheng, Yurong Qian, Jie He, Zerui Kang, and Lei Deng. Graph neural network with self-supervised learning for noncoding rna–drug resistance association prediction. *Journal of Chemical Information and Modeling*, 62(15):3676–3684, 2022.

[70] Jinhua Zhu, Yingce Xia, Lijun Wu, Shufang Xie, Wengang Zhou, Tao Qin, Houqiang Li, and Tie-Yan Liu. Dual-view molecular pre-training. In *Proceedings of the 29th ACM SIGKDD Conference on Knowledge Discovery and Data Mining*, pages 3615–3627, 2023.

Appendix Overview

- **Appendix A**: Related Work.
- **Appendix B**: Memory and Computational Constraints.
- **Appendix C**: Additional Experimental Information.
- **Appendix D**: Analysis of Noise in 3D Structures.
- **Appendix E**: Reproduction.
- **Appendix F**: Additional Results.

A Related Work

RNA property prediction RNA-specific models remain scarce, likely due to limited specialized datasets. Recent advancements in sequence modeling have shown promise, particularly with foundation models like RNA-FM [8], UTRBERT [66], and RINALMO [35], which use transformer-based architectures pre-trained on large RNA sequence corpora to predict various RNA functions and structures. While RNNs and CNNs have been applied to tasks like RNA methylation and protein binding [56], they struggle with long-range dependencies. Hybrid models like RNAdegformer [21], combining convolutional layers with self-attention, improve predictions by capturing both local and global dependencies. Although some efforts integrate 2D structures with transformers, explicit 2D and 3D geometric modeling for RNA remains underexplored, with graph-based models mainly focusing on RNA-protein and RNA-drug interaction tasks rather than property prediction [29, 65, 4, 69].

RNA structure prediction RNA 2D structure prediction has progressed from dynamic programming methods like Vienna RNAfold [23] to deep learning-based tools like SPOT-RNA2 [48] and UFold [16], which enhance accuracy by using neural networks and evolutionary data. Models such as E2Efold [9] and RNA-FM [8] employ transformer architectures to achieve state-of-the-art results in secondary structure prediction.

RNA 3D structure prediction has progressed through ab initio, template-based, and deep learning approaches. Ab initio methods (e.g., iFoldRNA [43], SimRNA [6]) balance detail and efficiency but struggle with non-canonical interactions. Template-based models (e.g., FARNA/FARFAR [10], 3dRNA [68]) depend on existing structures but are limited by available data. Deep learning models like DeepFoldRNA [34], RhoFold [45], RoseTTAFoldNA [5], and trRosettaRNA [57] show promise in predicting 3D structures from sequence data but face challenges with novel RNA families due to RNA's conformational flexibility [30].

Despite these advances, there is a gap in applying 2D and 3D modeling techniques to RNA property prediction. Most works focus on 1D representations and overlook the potential of geometric information from 2D and 3D structures. This study is the first to systematically explore the benefits and limitations of incorporating explicit structural data in deep learning-based RNA property prediction.

B Memory and Computational Constraints

In this section, we compare the models based on run times and GPU memory. Both Transformer1D2D and 3D models (even with nucleotide pooling) encounter out-of-memory (OOM) issues when processing longer sequences, such as those in the Fungal dataset (Table 1). This highlights the need for optimization to handle longer sequences. Figure 7 shows that Transformer1D scales poorly in both runtime and memory due to its expensive attention mechanism, and Transformer1D2D faces additional challenges by processing the sequence and adjacency matrix simultaneously. In contrast, simpler 2D models like GCN, GAT, and ChebNet are more efficient. 3D models also scale poorly with sequence length due to the increasing number of atoms. Overall, 2D models provide a good balance between computational demands and performance for encoding structural information.

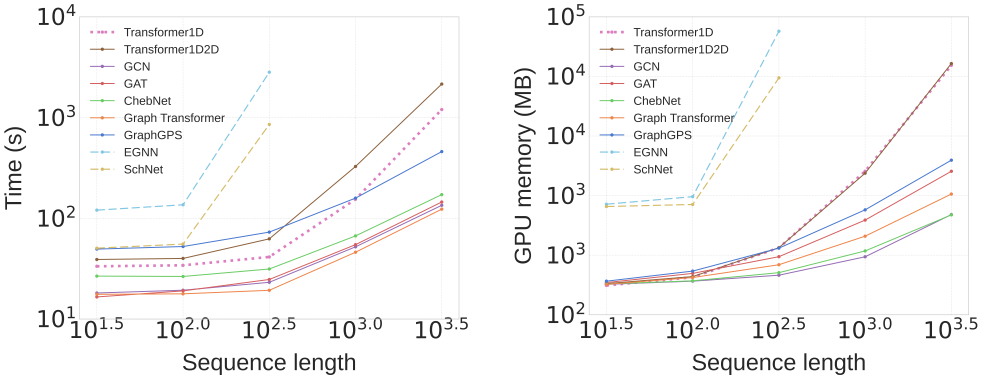

Figure 7: **Running time and memory usage comparison across models.** (1) Running time vs. sequence length (left): Transformer1D and Transformer1D2D scale poorly with sequence length due to expensive attention mechanisms and simultaneous processing of sequences and adjacency matrices, while simpler 2D models like GCN, GAT, and ChebNet are more efficient. (2) Memory usage vs. sequence length (right): Transformer1D2D and 3D models face out-of-memory issues with longer sequences, especially in the largest Fungal dataset, whereas 2D models use memory more efficiently, balancing computational demands and structural encoding.

C Additional Experimental Information

C.1 Dataset Statistics

Here, we present the statistics for each dataset used in the paper in Table 2. The datasets are categorized as small, medium, or large based on the number of sequences and sequence length. "Target" refers to the task the dataset is designed to predict, and "# Avg. Atoms" indicates the average number of atoms used in 3D models.

Table 2: The statistics of Tc-Riboswitches, Ribonanza, COVID, and Fungal datasets.

	Tc-Riboswitches	**Ribonanza**	**COVID**	**Fungal**
Dataset Size	Small	Medium	Medium	Large
Target	Switching Factor	Degradation	Degradation	Expression
# Sequences	355	2260	4082	7089
Sequence Length	66 - 75	177	107 - 130	150 - 3063
# Labels	1	2	3	1
# Avg. Atoms (for 3D models)	1531	3791	2598	N/A

C.2 Comparison of partial training data and partial sequence labeling

To clarify the differences and provide a more detailed explanation, we illustrate two experiments: partial training data and partial sequence labeling (Figure 8).

C.3 Details of noisy experiments: robustness and generalization

To create the noisy datasets, we vary the noise ratio r across the values $\{0.05, 0.1, 0.15, 0.2, 0.25, 0.3\}$. For each given noise ratio, we independently mutate the nucleotide at each position in a sequence with probability r, as illustrated in Figure 9. The resulting mutated sequence is then passed to the 2D and 3D prediction tools to generate the corresponding structures. Figure 4 gives a comprehensive illustration of getting noisy 1D, 2D, and 3D structures.

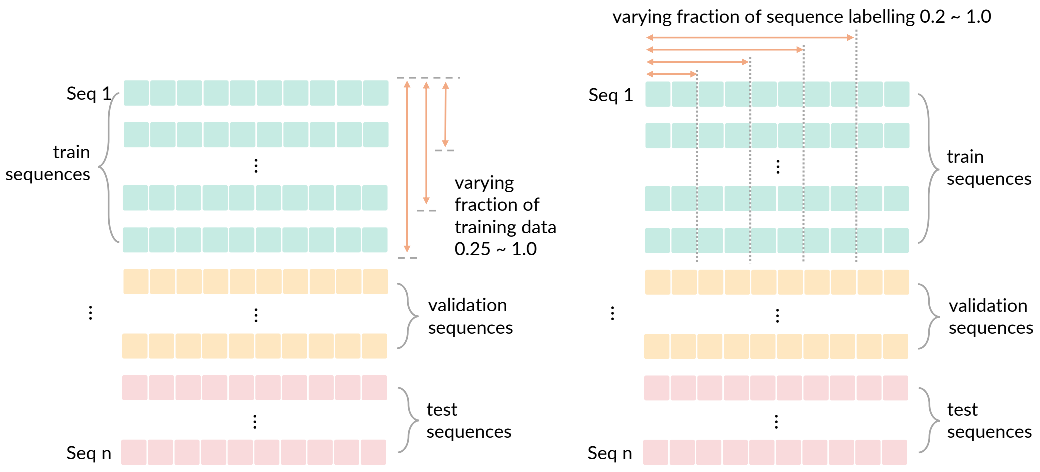

(a) Varying fraction of training data.

(b) Varying fraction of sequence labeling.

Figure 8: **Comparison of partial training data and partial sequence labeling.** The orange arrows indicate the varying components. (a) utilizes full nucleotide labels but trains on varying fractions of RNA sequences (0.25, 0.5, 0.75, 1.0). (b) uses all training sequences but with varying fractions of nucleotide labels (0.2, 0.4, 0.6, 0.8, 1.0). Therefore, (b) is only for nucleotide-level tasks.

For the robustness experiments, all training, validation, and testing are conducted on the noisy datasets. In contrast, for the generalization experiments, the model is trained and validated on clean datasets, and its performance is tested on noisy datasets with varying noise ratios.

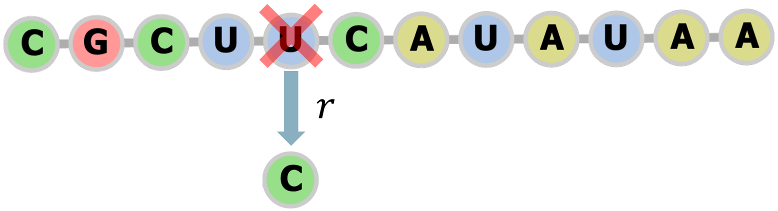

Figure 9: Mutation the nucleotide at each position independently with the probability r.

C.4 Analysis of Transformer1D and Transformer1D2D

To further validate that incorporating structural information contributes to the final results, we analyze the attention maps generated by Transformer1D and Transformer1D2D. Fig. 10 illustrates the average attention maps across all heads before the final output layer for both the models for a randomly selected RNA sequence. The attention maps of Transformer1D2D exhibit a striking similarity to both the adjacency matrix and the BPP matrix, whereas the attention maps from the standard Transformer model seem to suggest that the model does not learn to attend to the structural features. Moreover, we quantify this observation by computing the cosine similarity between the attention maps of the models and the true adjacency matrix and BPP for all sequences in the COVID dataset. The results, reported in Table 3 show that Transformer1D2D achieves much higher similarity scores compared to the 1D Transformer alone. This reinforces the conclusion that explicit encoding of structural information is essential for improved model performance.

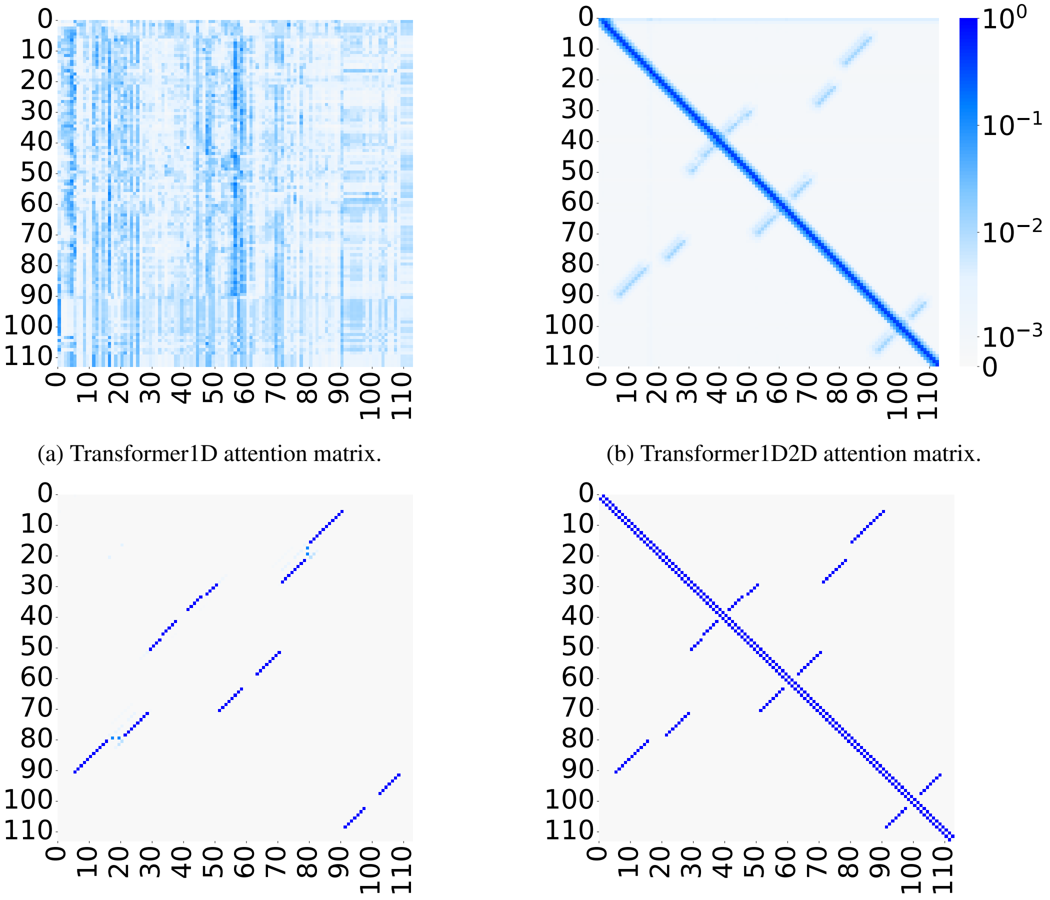

(a) Transformer1D attention matrix.

(b) Transformer1D2D attention matrix.

(c) Base pair probability matrix.

(d) Graph adjacency matrix.

Figure 10: **The heatmaps of matrices in Transformer1D and Transformer1D2D.** Attention maps from Transformer1D2D exhibit a striking resemblance to both the adjacency matrix and BPP matrix, highlighting the model's ability to learn structural features. In contrast, the standard Transformer struggles with this task, as shown by lower cosine similarity scores, reinforcing the conclusion that explicitly encoding structural information is crucial for enhanced model performance.

Table 3: **Cosine similarity values for different models.** Cosine similarity scores between the attention maps and the true adjacency and BPP matrices for all sequences in the COVID dataset demonstrate that Transformer1D2D significantly outperforms the standard Transformer. These results underscore the importance of explicitly encoding structural information for superior model performance.

Model	**Cosine similarity adjacency**	**Cosine similarity BPP**
Transformer1D	0.107	0.090
Transformer1D2D	0.448	0.672

D Analysis of Noise in 3D Structures

As mentioned in the main context, predicted 3D structures consistently exhibit noise. In this section, we analyze this issue from two perspectives: sensitivity to sequence length and variability across different prediction tools.

D.1 Impact of Sequence Length on 3D Structure Prediction Noise

To investigate the hypothesis that longer sequences result in greater noise in 3D structure predictions, we randomly selected a COVID and Tc-Riboswitches dataset sequence and generated structures using four state-of-the-art 3D structure prediction tools: RhoFold [45], RNAComposer [64], trRosetta [5], and SimRNA [6]. High variability among these predicted structures would indicate significant uncertainty in absolute atom positions. We quantified this noise by aligning the structures using the Kabsch algorithm [26] and computing the pairwise RMSD values, resulting in a 4x4 matrix showing structural deviations between each pair of tools (see Table 4). The observed pairwise RMSD values ranged from 16 to 45 Å for the COVID dataset and from 11 to 15 Å for the Tc-Riboswitches dataset, reflecting substantial variability and suggesting considerable noise in the 3D predictions. This level of structural inaccuracy likely contributes to the poorer performance of 3D models. However, we found that 3D models outperform 1D models for shorter sequences, such as those in the Tc-Riboswitches dataset (67 to 73 nucleotides long). This improved performance is due to the lower noise in 3D predictions for shorter sequences, a phenomenon supported by previous studies [32, 37] and also exhibited by the comparatively smaller RMSD values reported in Table 4 for Tc-Riboswitches dataset. The reduced complexity of shorter sequences allows 3D models to capture structural details more accurately, thereby enhancing performance and validating that accurate 3D structure encoding can outperform 1D models.

Table 4: **Pairwise RMSD values (in Å) between 3D structure prediction tools for the COVID dataset (left) and Tc-Riboswitches dataset (right).** The results indicate larger noise in predictions for longer COVID sequences.

COVID	RhoFold	trRosetta	SimRNA	Composer
RhoFold	0	39.05192	44.76146	45.45994
trRosetta	39.05192	0	22.54974	18.17359
SimRNA	44.76146	22.54974	0	16.73399
Composer	45.45994	18.17359	16.73399	0

Tc-Ribo	RhoFold	trRosetta	SimRNA	Composer
RhoFold	0	14.338	11.996	15.056
trRosetta	14.338	0	12.932	14.916
SimRNA	11.996	12.932	0	14.243
Composer	15.056	14.916	14.243	0

D.2 Impact of different 3D prediction tools

In this section, we demonstrate the significant differences in 3D structures predicted by various tools. We compare the 3D structure obtained from RhoFold [45], which serves as our default method, with those predicted by RNAComposer [64], trRosetta [5], and SimRNA [6]. Each structure is visualized side by side with RhoFold in Figure 11 to facilitate a more intuitive comparison. As observed, these structures predicted by each tool vary considerably.

E Reproduction

This section outlines the necessary details to reproduce all experiments discussed in this paper. The code will be made publicly available upon acceptance.

E.1 Training details

All experiments were conducted on a single NVIDIA A100 GPU. For each baseline, hyperparameters were optimized using Optuna [1], restricting the search to models with fewer than 10 million parameters that fit within the memory constraints of an 80GB NVIDIA A100 GPU. Most baseline implementations were sourced from PyTorch Geometric [13]. The Transformer1D model was

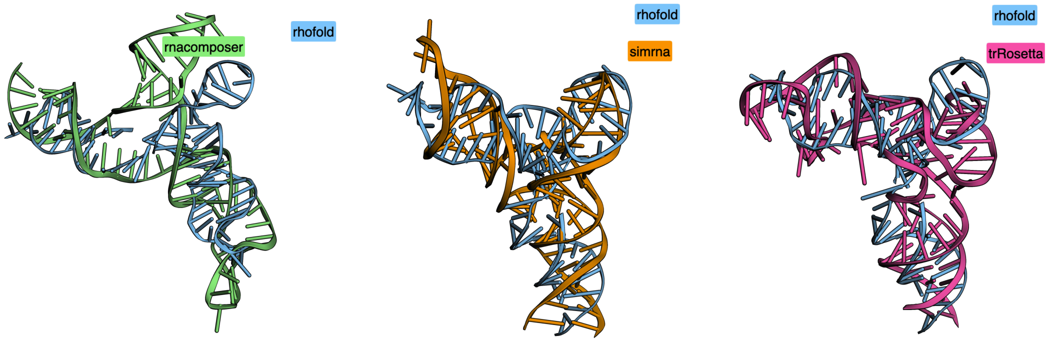

(a) RhoFold vs. RNAComposer (b) RhoFold vs. SimRNA (c) RhoFold vs. trRosetta

Figure 11: Comparison of RhoFold against other 3D structure prediction tools on an example sequence from Tc-Riboswitches dataset.

adapted to Transformer1D2D as detailed in the paper. For EGNN, we utilized the authors' implementation [40], and for SchNet, the implementation from [25] was used.

E.2 Hyperparameters

This section provides a comprehensive overview of the hyperparameters used in each baseline model, facilitating reproducibility and understanding of the model configurations.

Common hyperparameters across these models include `in_channels`, which specifies the number of input features, `hidden`, which determines the number of hidden units in each hidden layer, and `out_channels`, which defines the number of output features. The `L` parameter controls the number of layers in the network, and the `dropout` parameter sets the dropout rate for regularization. The `lr` parameter specifies the learning rate, and `weight_decay` sets the weight decay for regularization of the optimizer. For graph-level tasks, the `pool` parameter specifies the pooling method, which can be `mean`, `max`, or `add`.

Transformer1D is a standard Transformer architecture for RNA sequence processing. It includes an embedding layer to convert input tokens into dense vectors, positional encoding (PE) to retain sequence order, and a multi-layer Transformer encoder to capture complex dependencies within the sequence. There are some hyperparameters from the original transformer [54]. `nhead`, which defines the number of attention heads in each Transformer layer; `num_encoder_layers`, which controls the number of encoder layers in the Transformer; `d_model`, which determines the dimensionality of the embeddings and the model; `dim_feedforward`, which sets the dimensionality of the feedforward network model. To shrink the search space, we set `d_model` and `dim_feedforward` as the same with a new hyperparameter `hidden`.

Transformer1D2D is an adaptation of Transformer1D that integrates both sequence and 2D graph structure information. In addition to encoding each nucleotide, the model incorporates base pair probabilities (BPP) features for each nucleotide. It combines a standard Transformer with positional encoding and a convolutional layer applied to the graph adjacency matrix. This convolutional output is added to the Transformer's attention matrix, allowing the model to incorporate graph structure into its attention mechanism. This design captures both the sequential and structural dependencies in RNA data, improving predictive performance. The unique hyperparameter for this model is `kernel_size`, which specifies the size of the convolutional kernel.

GAT includes the unique hyperparameters `gat_heads`, which specify the number of attention heads in each GAT layer.

ChebNet model has the unique hyperparameter `power`, which specifies the polynomial order for the Chebyshev convolution.

GraphGPS and **Graph Transformer** includes `heads`, which specifies the number of attention heads in each layer, and `pe_dim`, which defines the dimensionality of positional encoding.

EGNN and **SchNet** are 3D models that operate at two granularities within the network: atom layers and nucleotide layers. The two types of layers are connected through nucleotide pooling. Atom layers use atoms as nodes, while nucleotide layers use nucleotides as nodes. Both the atom layer and nucleotide layer employ a point cloud setting and calculate edges based on the distance between two nodes. An edge is considered to exist if the distance is smaller than a certain threshold. Therefore, EGNN and SchNet share the following hyperparameters: `L_atom`, which denotes the number of atom layers; `L_nt`, which specifies the number of nucleotide layers; `threshold_atom`, which is the threshold for edges in atom layers; and `threshold_nt`, which is the threshold for edges in nucleotide layers.

For SchNet, the unique hyperparameters include `num_filters`, which refers to the number of filters used in convolutional layers, and `num_gaussians`, which indicates the number of Gaussian functions used for radial filters. For a more detailed explanation of these hyperparameters, please refer to [42].

To ensure a fair comparison, the best hyperparameter configuration for each method was selected based on validation set performance. We report the mean performance and standard deviation across 5 random splits on the test set. For the COVID and Ribonanza datasets, we performed hyperparameter searching only on the COVID dataset and applied the same configuration to Ribonanza, as the two datasets share similar properties. The optimal hyperparameters are shown in Table 5.

F Additional Results

In this section, we present the additional results supporting Figures 2, 3, 5, and 6 in main text.

F.1 Impact of data availability

The detailed results of partial training data from Figure 2 are shown in Tables 6, 7, and 8.

F.2 Impact of partial labeling

The detailed results of the partial labeling sequence from Figure 3 are shown in Tables 9 and 10.

F.3 Robustness to sequencing noise

The results of the robustness experiment from Figure 5 are shown in Tables 11, 12, 13, and 14.

F.4 Generalization to OOD data

The results of the generalization experiment from Figure 6 are shown in Tables 15, 16, 17, and 18.

	Hyperparameter	COVID & Ribonanza	Tc-riboswitches	Fungal
Transformer1D	lr	0.001	0.0005	0.001
	weight_decay	0	0.0005	0.0005
	hidden	128	64	32
	nhead	8	8	8
	num_encoder_layers	8	6	6
	pool	/	mean	mean
Transformer1D2D	lr	0.001	0.005	OOM
	weight_decay	0	0	
	hidden	256	32	
	nhead	16	4	
	num_encoder_layers	8	4	
	pool	mean	mean	
	kernel_size	5	5	
GCN	lr	0.001	0.0001	0.0001
	weight_decay	0	0	0
	hidden	1024	512	512
	L	7	5	3
	dropout	0.3	0.1	0.7
	pool	/	max	add
ChebNet	lr	0.001	0.005	0.0001
	weight_decay	0	0.0005	0
	hidden	512	256	256
	L	5	7	5
	dropout	0.3	0.3	0.3
	power	6	2	2
	pool	/	max	mean
GAT	lr	0.001	0.005	0.0005
	weight_decay	0	0	0.0005
	hidden	256	1024	256
	L	7	3	7
	dropout	0.1	0.1	0.3
	heads	4	2	1
	pool	/	add	add
Graph Transformer	lr	0.001	0.005	0.005
	weight_decay	0	0	0.0005
	hidden	128	64	256
	L	7	5	7
	heads	4	1	2
	pool	/	add	mean
GraphGPS	lr	0.001	1e-5	0.0005
	weight_decay	0	0.0005	0.0005
	hidden	256	256	512
	L	5	7	5
	heads	2	1	2
	pool	/	add	max
EGNN	lr	0.0005	0.001	OOM
	weight_decay	0	0	
	hidden	256	256	
	L_atom	3	3	
	L_nt	2	1	
	threshold_atom	1.6	1.6	
	threshold_nt	22	22	
SchNet	lr	0.0005	0.001	OOM
	weight_decay	0	0	
	hidden	128	128	
	L_atom	1	1	
	L_nt	2	4	
	threshold_atom	1.6	1.8	
	threshold_nt	44	88	
	num_filters	128	256	
	num_gaussians	50	50	

Table 5: Best hyperparameters for each model and dataset. Hyperparameters are searched by Optuna. COVID and Ribonanza share the same hyperparameters.

Table 6: Performance (MCRMSE) of different models across various training data (mean ± standard deviation) fractions on COVID dataset.

COVID	**0.25**	**0.50**	**0.75**	**1.00**
Transformer1D	0.429 ± 0.018	0.410 ± 0.016	0.375 ± 0.018	0.361 ± 0.017
Transformer1D2D	0.345 ± 0.010	0.330 ± 0.011	0.306 ± 0.014	0.305 ± 0.012
GCN	0.389 ± 0.008	0.377 ± 0.009	0.358 ± 0.014	0.359 ± 0.009
GAT	0.352 ± 0.011	0.342 ± 0.009	0.320 ± 0.014	0.315 ± 0.006
ChebNet	0.320 ± 0.011	0.309 ± 0.009	0.286 ± 0.018	0.279 ± 0.007
Graph Transformer	0.356 ± 0.008	0.344 ± 0.007	0.324 ± 0.016	0.318 ± 0.008
GraphGPS	0.367 ± 0.018	0.362 ± 0.005	0.344 ± 0.010	0.332 ± 0.013
EGNN	0.398 ± 0.001	0.391 ± 0.013	0.368 ± 0.013	0.364 ± 0.003
SchNet	0.419 ± 0.003	0.414 ± 0.011	0.392 ± 0.011	0.390 ± 0.006

Table 7: Performance (MCRMSE) of different models across various fractions of training data (mean ± standard deviation) on Ribonanza dataset.

Ribonanza	**0.25**	**0.50**	**0.75**	**1.00**
Transformer1D	0.777 ± 0.014	0.740 ± 0.005	0.739 ± 0.001	0.705 ± 0.015
Transformer1D2D	0.630 ± 0.016	0.553 ± 0.015	0.541 ± 0.018	0.514 ± 0.004
GCN	0.668 ± 0.018	0.618 ± 0.017	0.612 ± 0.013	0.595 ± 0.006
GAT	0.600 ± 0.018	0.553 ± 0.026	0.544 ± 0.012	0.534 ± 0.006
ChebNet	0.537 ± 0.019	0.494 ± 0.022	0.499 ± 0.007	0.468 ± 0.002
Graph Transformer	0.567 ± 0.019	0.529 ± 0.013	0.529 ± 0.010	0.515 ± 0.001
GraphGPS	0.581 ± 0.021	0.529 ± 0.015	0.540 ± 0.004	0.523 ± 0.003
EGNN	0.694 ± 0.010	0.650 ± 0.010	0.632 ± 0.015	0.619 ± 0.007
SchNet	0.768 ± 0.008	0.724 ± 0.013	0.715 ± 0.015	0.685 ± 0.006

Table 8: Performance (MCRMSE) of different models across various fractions of training data (mean ± standard deviation) on Fungal dataset.

Fungal	**0.25**	**0.50**	**0.75**	**1.00**
Transformer1D	1.510 ± 0.006	1.446 ± 0.014	1.475 ± 0.035	1.417 ± 0.005
GCN	1.243 ± 0.064	1.244 ± 0.128	1.151 ± 0.077	1.192 ± 0.077
GAT	1.211 ± 0.125	1.168 ± 0.033	1.146 ± 0.109	1.112 ± 0.035
ChebNet	1.125 ± 0.097	1.011 ± 0.010	1.008 ± 0.009	0.973 ± 0.003
Graph Transformer	1.415 ± 0.014	1.331 ± 0.163	1.306 ± 0.127	1.317 ± 0.002
GraphGPS	1.289 ± 0.071	1.377 ± 0.127	1.357 ± 0.106	1.025 ± 0.081

Table 9: Performance (MCRMSE) of different models across various fractions of sequence labeling (mean ± standard deviation) on COVID dataset.

COVID	**0.2**	**0.4**	**0.6**	**0.8**	**1.0**
Transformer1D	0.654 ± 0.040	0.559 ± 0.011	0.480 ± 0.004	0.429 ± 0.034	0.361 ± 0.017
Transformer1D2D	0.502 ± 0.002	0.470 ± 0.052	0.374 ± 0.007	0.325 ± 0.006	0.305 ± 0.012
GCN	0.450 ± 0.012	0.416 ± 0.012	0.397 ± 0.012	0.378 ± 0.011	0.359 ± 0.009
GAT	0.411 ± 0.010	0.376 ± 0.012	0.360 ± 0.012	0.336 ± 0.009	0.315 ± 0.006
ChebNet	0.380 ± 0.007	0.344 ± 0.008	0.325 ± 0.009	0.299 ± 0.007	0.279 ± 0.007
Graph Transformer	0.415 ± 0.012	0.379 ± 0.011	0.362 ± 0.011	0.338 ± 0.004	0.318 ± 0.008
GraphGPS	0.428 ± 0.015	0.400 ± 0.017	0.376 ± 0.013	0.351 ± 0.007	0.332 ± 0.013
EGNN	0.436 ± 0.014	0.421 ± 0.010	0.407 ± 0.004	0.385 ± 0.006	0.364 ± 0.003
SchNet	0.442 ± 0.004	0.429 ± 0.005	0.413 ± 0.001	0.407 ± 0.005	0.390 ± 0.006

Table 10: Performance (MCRMSE) of different models across various fractions of sequence labeling (mean ± standard deviation) on Ribonanza dataset.

Ribonanza	**0.2**	**0.4**	**0.6**	**0.8**	**1.0**
Transformer1D	1.137 ± 0.163	0.929 ± 0.023	0.823 ± 0.018	0.742 ± 0.013	0.705 ± 0.015
Transformer1D2D	0.859 ± 0.025	0.638 ± 0.013	0.632 ± 0.028	0.568 ± 0.013	0.514 ± 0.004
GCN	1.191 ± 0.031	1.026 ± 0.079	1.111 ± 0.206	1.070 ± 0.137	0.595 ± 0.006
GAT	0.703 ± 0.015	0.632 ± 0.025	0.612 ± 0.030	0.560 ± 0.010	0.534 ± 0.006
ChebNet	0.614 ± 0.013	0.546 ± 0.008	0.540 ± 0.008	0.514 ± 0.006	0.468 ± 0.002
Graph Transformer	0.719 ± 0.043	0.607 ± 0.020	0.584 ± 0.015	0.552 ± 0.013	0.515 ± 0.001
GraphGPS	0.743 ± 0.058	0.663 ± 0.026	0.627 ± 0.024	0.651 ± 0.026	0.523 ± 0.003
EGNN	0.882 ± 0.010	0.722 ± 0.021	0.687 ± 0.008	0.665 ± 0.013	0.619 ± 0.007
SchNet	0.810 ± 0.002	0.781 ± 0.009	0.750 ± 0.009	0.725 ± 0.004	0.685 ± 0.006

Table 11: Performance (MCRMSE) of various models in **robustness** experiments on the **COVID** dataset (mean ± standard deviation).

Model	**0.00**	**0.05**	**0.10**	**0.15**	**0.20**	**0.25**	**0.30**
Transformer1D	0.361 ± 0.017	0.386 ± 0.015	0.400 ± 0.010	0.409 ± 0.006	0.428 ± 0.005	0.435 ± 0.003	0.449 ± 0.011
Transformer1D2D	0.305 ± 0.012	0.373 ± 0.007	0.403 ± 0.007	0.428 ± 0.011	0.444 ± 0.015	0.457 ± 0.009	0.463 ± 0.009
GCN	0.359 ± 0.009	0.436 ± 0.009	0.464 ± 0.011	0.481 ± 0.010	0.491 ± 0.012	0.497 ± 0.009	0.501 ± 0.009
GAT	0.315 ± 0.006	0.409 ± 0.009	0.448 ± 0.011	0.471 ± 0.010	0.484 ± 0.012	0.494 ± 0.011	0.500 ± 0.010
ChebNet	0.279 ± 0.007	0.368 ± 0.003	0.423 ± 0.009	0.456 ± 0.007	0.471 ± 0.009	0.481 ± 0.010	0.487 ± 0.008
Graph Transformer	0.318 ± 0.008	0.403 ± 0.008	0.441 ± 0.012	0.467 ± 0.011	0.480 ± 0.012	0.487 ± 0.010	0.494 ± 0.011
GraphGPS	0.332 ± 0.013	0.408 ± 0.012	0.441 ± 0.010	0.464 ± 0.014	0.475 ± 0.012	0.484 ± 0.012	0.487 ± 0.008
EGNN	0.364 ± 0.003	0.432 ± 0.012	0.467 ± 0.009	0.486 ± 0.009	0.499 ± 0.011	0.505 ± 0.012	0.511 ± 0.011
SchNet	0.390 ± 0.006	0.447 ± 0.012	0.477 ± 0.011	0.496 ± 0.009	0.507 ± 0.014	0.513 ± 0.012	0.517 ± 0.010

Table 12: Performance (MCRMSE) of various models in **robustness** experiments on the **Ribonanza** dataset (mean ± standard deviation).

Model	**0.00**	**0.05**	**0.10**	**0.15**	**0.20**	**0.25**	**0.30**
Transformer1D	0.705 ± 0.015	0.733 ± 0.010	0.769 ± 0.014	0.782 ± 0.005	0.794 ± 0.010	0.805 ± 0.017	0.823 ± 0.005
Transformer1D2D	0.514 ± 0.004	0.635 ± 0.004	0.714 ± 0.014	0.763 ± 0.008	0.790 ± 0.009	0.811 ± 0.014	0.830 ± 0.008
GCN	0.595 ± 0.006	0.750 ± 0.014	0.846 ± 0.008	0.893 ± 0.003	0.912 ± 0.005	0.924 ± 0.005	0.929 ± 0.005
GAT	0.534 ± 0.006	0.691 ± 0.015	0.785 ± 0.006	0.850 ± 0.003	0.877 ± 0.001	0.904 ± 0.007	0.915 ± 0.007
ChebNet	0.468 ± 0.002	0.611 ± 0.012	0.720 ± 0.006	0.802 ± 0.011	0.841 ± 0.003	0.876 ± 0.007	0.897 ± 0.008
Graph Transformer	0.515 ± 0.001	0.670 ± 0.011	0.768 ± 0.011	0.833 ± 0.008	0.870 ± 0.006	0.893 ± 0.010	0.908 ± 0.007
GraphGPS	0.523 ± 0.003	0.677 ± 0.017	0.772 ± 0.006	0.832 ± 0.006	0.872 ± 0.004	0.896 ± 0.011	0.912 ± 0.006
EGNN	0.619 ± 0.007	0.764 ± 0.003	0.847 ± 0.003	0.889 ± 0.005	0.904 ± 0.003	0.917 ± 0.000	0.922 ± 0.002
SchNet	0.685 ± 0.006	0.814 ± 0.006	0.873 ± 0.004	0.897 ± 0.004	0.908 ± 0.004	0.918 ± 0.005	0.922 ± 0.005

Table 13: Performance (MCRMSE) of various models in **robustness** experiments on the **Fungal** dataset (mean ± standard deviation).

Model	**0.00**	**0.05**	**0.10**	**0.15**	**0.20**	**0.25**	**0.30**
Transformer1D	1.417 ± 0.005	1.545 ± 0.045	1.546 ± 0.044	1.546 ± 0.046	1.543 ± 0.048	1.543 ± 0.051	1.550 ± 0.041
GCN	1.192 ± 0.077	1.222 ± 0.044	1.255 ± 0.002	1.277 ± 0.014	1.269 ± 0.011	1.328 ± 0.026	1.294 ± 0.025
GAT	1.112 ± 0.035	1.244 ± 0.074	1.391 ± 0.155	1.334 ± 0.099	1.468 ± 0.056	1.444 ± 0.094	1.446 ± 0.092
ChebNet	0.978 ± 0.000	1.031 ± 0.003	1.091 ± 0.007	1.108 ± 0.009	1.243 ± 0.005	1.210 ± 0.014	1.269 ± 0.007
Graph Transformer	1.342 ± 0.087	1.267 ± 0.116	1.409 ± 0.046	1.426 ± 0.051	1.442 ± 0.038	1.413 ± 0.020	1.450 ± 0.018
GraphGPS	1.083 ± 0.131	1.048 ± 0.095	1.133 ± 0.057	1.109 ± 0.040	1.173 ± 0.071	1.256 ± 0.016	1.328 ± 0.041

Table 14: Performance (MCRMSE) of various models in **robustness** experiments on the **Tc-riboswitches** dataset (mean ± standard deviation).

Model	**0.00**	**0.05**	**0.10**	**0.15**	**0.20**	**0.25**	**0.30**
Transformer1D	0.705 ± 0.079	0.698 ± 0.071	0.736 ± 0.004	0.672 ± 0.003	0.739 ± 0.008	0.694 ± 0.011	0.675 ± 0.047
Transformer1D2D	0.633 ± 0.001	0.697 ± 0.031	0.742 ± 0.003	0.708 ± 0.008	0.681 ± 0.001	0.762 ± 0.022	0.738 ± 0.016
GCN	0.701 ± 0.004	0.758 ± 0.003	0.747 ± 0.005	0.744 ± 0.004	0.733 ± 0.013	0.740 ± 0.011	0.765 ± 0.009
GAT	0.685 ± 0.024	0.749 ± 0.017	0.770 ± 0.047	0.734 ± 0.021	0.737 ± 0.009	0.753 ± 0.001	0.747 ± 0.011
ChebNet	0.621 ± 0.022	0.766 ± 0.014	0.754 ± 0.021	0.738 ± 0.014	0.763 ± 0.039	0.778 ± 0.048	0.739 ± 0.004
Graph Transformer	0.703 ± 0.054	0.754 ± 0.005	0.754 ± 0.006	0.773 ± 0.008	0.810 ± 0.087	0.742 ± 0.004	0.754 ± 0.005
GraphGPS	0.702 ± 0.028	0.785 ± 0.053	0.805 ± 0.092	0.750 ± 0.006	0.755 ± 0.060	0.769 ± 0.031	1.078 ± 0.469
EGNN	0.663 ± 0.010	0.750 ± 0.001	0.739 ± 0.002	0.749 ± 0.005	0.749 ± 0.001	0.749 ± 0.001	0.756 ± 0.013
SchNet	0.655 ± 0.038	0.762 ± 0.005	0.742 ± 0.002	0.771 ± 0.037	0.746 ± 0.005	0.791 ± 0.016	0.730 ± 0.016

Table 15: Performance (MCRMSE) of various models in **generalization** experiments on the **COVID** dataset (mean ± standard deviation).

Model	**0.00**	**0.05**	**0.10**	**0.15**	**0.20**	**0.25**	**0.30**
Transformer1D	0.361 ± 0.017	0.382 ± 0.022	0.402 ± 0.018	0.436 ± 0.015	0.461 ± 0.021	0.478 ± 0.015	0.494 ± 0.016
Transformer1D2D	0.305 ± 0.012	0.406 ± 0.016	0.466 ± 0.017	0.513 ± 0.016	0.545 ± 0.027	0.581 ± 0.025	0.596 ± 0.018
GCN	0.359 ± 0.009	0.459 ± 0.011	0.508 ± 0.011	0.550 ± 0.014	0.572 ± 0.016	0.601 ± 0.014	0.612 ± 0.008
GAT	0.315 ± 0.006	0.437 ± 0.013	0.490 ± 0.013	0.528 ± 0.008	0.555 ± 0.013	0.580 ± 0.015	0.592 ± 0.012
ChebNet	0.279 ± 0.007	0.415 ± 0.017	0.483 ± 0.023	0.538 ± 0.025	0.571 ± 0.029	0.604 ± 0.030	0.621 ± 0.028
Graph Transformer	0.318 ± 0.008	0.449 ± 0.015	0.501 ± 0.018	0.543 ± 0.015	0.571 ± 0.019	0.596 ± 0.014	0.609 ± 0.014
GraphGPS	0.332 ± 0.013	0.443 ± 0.011	0.496 ± 0.006	0.536 ± 0.005	0.559 ± 0.010	0.586 ± 0.007	0.593 ± 0.005
EGNN	0.365 ± 0.011	0.458 ± 0.014	0.504 ± 0.018	0.530 ± 0.020	0.549 ± 0.021	0.565 ± 0.022	0.572 ± 0.022
SchNet	0.390 ± 0.006	0.457 ± 0.011	0.491 ± 0.008	0.515 ± 0.007	0.531 ± 0.010	0.543 ± 0.009	0.556 ± 0.002

Table 16: Performance (MCRMSE) of various models in **generalization** experiments on the **Ribonanza** dataset (mean ± standard deviation).

Model	**0.00**	**0.05**	**0.10**	**0.15**	**0.20**	**0.25**	**0.30**
Transformer1D	0.705 ± 0.015	0.747 ± 0.005	0.796 ± 0.006	0.828 ± 0.008	0.860 ± 0.013	0.886 ± 0.013	0.899 ± 0.003
Transformer1D2D	0.514 ± 0.004	0.685 ± 0.014	0.857 ± 0.008	0.986 ± 0.015	1.055 ± 0.007	1.142 ± 0.020	1.192 ± 0.034
GCN	0.595 ± 0.006	0.857 ± 0.018	0.993 ± 0.012	1.054 ± 0.034	1.094 ± 0.043	1.129 ± 0.061	1.139 ± 0.075
GAT	0.534 ± 0.006	0.778 ± 0.021	0.919 ± 0.030	1.003 ± 0.056	1.047 ± 0.073	1.076 ± 0.082	1.093 ± 0.091
ChebNet	0.468 ± 0.002	0.699 ± 0.005	0.881 ± 0.038	1.025 ± 0.095	1.083 ± 0.111	1.165 ± 0.185	1.200 ± 0.220
Graph Transformer	0.515 ± 0.001	0.752 ± 0.005	0.930 ± 0.013	1.067 ± 0.036	1.124 ± 0.033	1.194 ± 0.080	1.224 ± 0.104
GraphGPS	0.523 ± 0.003	0.771 ± 0.026	0.958 ± 0.068	1.087 ± 0.142	1.116 ± 0.195	1.154 ± 0.202	1.165 ± 0.196
EGNN	0.691 ± 0.006	0.815 ± 0.004	0.975 ± 0.026	1.138 ± 0.078	1.228 ± 0.079	1.350 ± 0.173	1.395 ± 0.187
SchNet	0.685 ± 0.006	0.844 ± 0.006	0.949 ± 0.022	1.068 ± 0.035	1.157 ± 0.069	1.270 ± 0.049	1.342 ± 0.117

Table 17: Performance (MCRMSE) of various models in **generalization** experiments on the **Fungal** dataset (mean ± standard deviation).

Model	**0.00**	**0.05**	**0.10**	**0.15**	**0.20**	**0.25**	**0.30**
Transformer1D	1.417 ± 0.005	1.575 ± 0.002	1.575 ± 0.002	1.575 ± 0.002	1.575 ± 0.002	1.575 ± 0.002	1.575 ± 0.002
GCN	1.192 ± 0.077	1.230 ± 0.061	1.256 ± 0.050	1.280 ± 0.052	1.290 ± 0.044	1.328 ± 0.032	1.333 ± 0.046
GAT	1.112 ± 0.035	1.262 ± 0.115	1.284 ± 0.102	1.312 ± 0.092	1.334 ± 0.087	1.364 ± 0.080	1.373 ± 0.072
ChebNet	0.973 ± 0.003	1.118 ± 0.008	1.257 ± 0.018	1.382 ± 0.022	1.525 ± 0.020	1.686 ± 0.030	1.777 ± 0.033
Graph Transformer	1.317 ± 0.002	1.407 ± 0.053	1.418 ± 0.046	1.427 ± 0.040	1.439 ± 0.033	1.447 ± 0.029	1.456 ± 0.028
GraphGPS	1.025 ± 0.081	1.083 ± 0.011	1.160 ± 0.006	1.217 ± 0.012	1.316 ± 0.026	1.405 ± 0.040	1.463 ± 0.052

Table 18: Performance (MCRMSE) of various models in **generalization** experiments on the **Tc-riboswitches** dataset (mean ± standard deviation).

Model	**0.00**	**0.05**	**0.10**	**0.15**	**0.20**	**0.25**	**0.30**
Transformer1D	0.705 ± 0.079	0.711 ± 0.038	0.732 ± 0.007	0.753 ± 0.019	0.815 ± 0.091	0.803 ± 0.062	0.796 ± 0.079
Transformer1D2D	0.633 ± 0.001	0.705 ± 0.007	0.745 ± 0.008	0.749 ± 0.017	0.800 ± 0.034	0.766 ± 0.017	0.754 ± 0.014
GCN	0.701 ± 0.004	0.774 ± 0.026	0.781 ± 0.051	0.782 ± 0.062	0.825 ± 0.093	0.845 ± 0.072	0.858 ± 0.126
GAT	0.685 ± 0.024	0.829 ± 0.074	0.958 ± 0.131	0.926 ± 0.152	1.037 ± 0.297	0.998 ± 0.213	1.036 ± 0.392
ChebNet	0.621 ± 0.022	0.824 ± 0.185	0.862 ± 0.251	0.888 ± 0.302	0.997 ± 0.439	0.983 ± 0.412	1.045 ± 0.514
Graph Transformer	0.710 ± 0.041	0.759 ± 0.035	0.770 ± 0.047	0.776 ± 0.054	0.815 ± 0.101	0.795 ± 0.085	0.822 ± 0.115
GraphGPS	0.715 ± 0.012	0.751 ± 0.016	0.801 ± 0.023	0.795 ± 0.014	0.833 ± 0.025	0.814 ± 0.022	0.830 ± 0.018
EGNN	0.663 ± 0.010	0.760 ± 0.043	0.898 ± 0.134	0.901 ± 0.123	0.849 ± 0.053	1.058 ± 0.239	1.192 ± 0.453
SchNet	0.655 ± 0.038	1.368 ± 0.449	1.099 ± 0.320	1.419 ± 0.491	0.900 ± 0.119	1.957 ± 0.858	2.025 ± 0.779